PHYSICAL REVIEW D **95,** 014510 (2017)

Pion-nucleon scattering in the Roper channel from lattice QCD

C. B. Lang,[1,*] L. Leskovec,[2,†] M. Padmanath,[1,3,‡] and S. Prelovsek[4,5,3,6,§]

[1]*Institute of Physics, University of Graz, A-8010 Graz, Austria*
[2]*Department of Physics, University of Arizona, Tucson, Arizona 85721, USA*
[3]*Institut für Theoretische Physik, Universität Regensburg, D-93040 Regensburg, Germany*
[4]*Department of Physics, University of Ljubljana, 1000 Ljubljana, Slovenia*
[5]*Jozef Stefan Institute, 1000 Ljubljana, Slovenia*
[6]*Theory Center, Jefferson Lab, 12000 Jefferson Avenue, Newport News, Virginia 23606, USA*

(Received 12 October 2016; published 31 January 2017)

We present a lattice QCD study of $N\pi$ scattering in the positive-parity nucleon channel, where the puzzling Roper resonance $N^*(1440)$ resides in experiment. The study is based on the PACS-CS ensemble of gauge configurations with $N_f = 2 + 1$ Wilson-clover dynamical fermions, $m_\pi \simeq 156$ MeV and $L \simeq 2.9$ fm. In addition to a number of qqq interpolating fields, we implement operators for $N\pi$ in p-wave and $N\sigma$ in s-wave. In the center-of-momentum frame we find three eigenstates below 1.65 GeV. They are dominated by $N(0)$, $N(0)\pi(0)\pi(0)$ [mixed with $N(0)\sigma(0)$] and $N(p)\pi(-p)$ with $p \simeq 2\pi/L$, where momenta are given in parentheses. This is the first simulation where the expected multi-hadron states are found in this channel. The experimental $N\pi$ phase shift would—in the approximation of purely elastic $N\pi$ scattering—imply an additional eigenstate near the Roper mass $m_R \simeq 1.43$ GeV for our lattice size. We do not observe any such additional eigenstate, which indicates that $N\pi$ elastic scattering alone does not render a low-lying Roper. Coupling with other channels, most notably with $N\pi\pi$, seems to be important for generating the Roper resonance, reinforcing the notion that this state could be a dynamically generated resonance. Our results are in line with most of the previous lattice studies based just on qqq interpolators, which did not find a Roper eigenstate below 1.65 GeV. The study of the coupled-channel scattering including a three-particle decay $N\pi\pi$ remains a challenge.

DOI: 10.1103/PhysRevD.95.014510

I. INTRODUCTION

Pion-nucleon scattering in the $J^P = 1/2^+$ channel captures the information on the excitations of the nucleon ($N = p$, n). The $N\pi$ scattering in p-wave is elastic only below the inelastic threshold $m_N + 2m_\pi$ for $N\pi\pi$. The main feature in this channel at low energies is the so-called Roper resonance with $m_R = (1.41\text{–}1.45)$ GeV and $\Gamma_R = (0.25\text{–}0.45)$ GeV [1] that was first introduced by Roper [2] to describe the experimental $N\pi$ scattering. The resonance decays to $N\pi$ in p-wave with a branching ratio Br $\simeq$ 55%–75% and to $N\pi\pi$ with Br $\simeq$ 30%–40% [including $N(\pi\pi)^{I=0}_{s\text{-wave}}$, $\Delta\pi$ and $N\rho$], while isospin-breaking and electromagnetic decays lead to a Br well below one percent.

Phenomenological approaches that considered the $N^*(1440)$ resonance as a dominantly qqq state, for example quark models [3–5], gave a mass that is too high and a width that is too small in comparison to experiment. This led to several suggestions on its nature and a large number of phenomenological studies. One possibility is a dynamically generated Roper resonance where the coupled-channel scattering $N\pi/N\sigma/\Delta\pi$ describes the $N\pi$ experimental scattering data without any excited qqq core [6–9]. The scenarios with significant $qqqq\bar{q}$ Fock components [10,11] and hybrids $qqqG$ with gluon excitations [12,13] were also explored. The excited qqq core, where the interaction of quarks is supplemented by the pion exchange, brings the mass closer to experiment [14,15]. A similar effect is found as a result of some other mechanisms that accompany the qqq core, for example a vibrating $\pi\sigma$ contribution [16] or coupling to all allowed channels [17]. These models are not directly based on QCD, while the effective field theories contain a large number of low-energy constants that need to be determined by other means. The rigorous Roy-Steiner approach is based on phase shift data and dispersion relations implementing unitarity, analyticity and crossing symmetry; it leads to $N\pi$ scattering amplitudes at energies $E \leq 1.38$ GeV that do not cover the whole region of the Roper resonance [18]. The implications of the present simulation on various scenarios are discussed in Sec. IV.

All previous lattice QCD simulations, except for [19], addressed excited states in this channel using three-quark operators; this has conceptual issues for a strongly decaying resonance where coupling to multi-hadron states is essential. In principle multi-hadron eigenstates can also arise from the qqq interpolators in a dynamical lattice QCD simulation but in practical calculations the coupling to qqq

*christian.lang@uni-graz.at
†leskovec@email.arizona.edu
‡Padmanath.Madanagopalan@physik.uni-regensburg.de
§sasa.prelovsek@ijs.si

was too weak for an effect. Another assumption of the simple operator approach is that the energy of the first excited eigenstate is identified with the mass of $N^*(1440)$, which is a drastic approximation for a wide resonance. The more rigorous Lüscher approach [20,21] assuming elastic scattering predicts an eigenstate in the energy region within the resonance width (see Fig. 7).

The masses of the Roper obtained in the recent dynamical lattice simulations [22–28] using the qqq approach are summarized in [29]. Extrapolating these to physical quark masses, where $m_{u/d} \simeq m_{u/d}^{\text{phys}}$, the Roper mass was found above 1.65 GeV by all dynamical studies except [22], so most of the studies disfavor a low-lying Roper qqq core. The only dynamical study that observes a mass around 1.4 GeV was done by the χQCD collaboration [22]; it was based on the fermions with good chiral properties (domain-wall sea quarks and overlap valence quarks) and employed a sequential empirical Bayesian (SEB) method to extract eigenenergies from a single correlator. It is not yet finally settled [22,29–31] whether the discrepancy of [22] with other results is related to the chiral properties of quarks, use of SEB or poor variety of interpolator spatial widths in some studies.[1] Linear combinations of operators with different spatial widths allow to form the radially excited eigenstate with a node in the radial wave function, which was found at $r \simeq 0.8$ fm in [22,28,32].

An earlier quenched simulation [33] based on qqq interpolators used overlap fermions and the SEB method to extract eigenenergies. The authors find a crossover between first excited $1/2^+$ state and ground $1/2^-$ state as a function of the quark mass, approaching the experimental situation. A more recent quenched calculation [34] using Fat link irrelevant clover (FLIC) fermions with improved chiral properties and variational approach also reported a similar observation.

In continuum the $N^*(1440)$ is not an asymptotic state but a strongly decaying resonance that manifests itself in the continuum of $N\pi$ and $N\pi\pi$ states. The spectrum of those states becomes discrete on the finite lattice of size L. For noninteracting N and π the periodic boundary conditions in space constrain the momenta to multiples of $2\pi/L$. The interactions modify the energies of these discrete multi-hadron states and possibly render additional eigenstates.

The multi-hadron states have never been established in the previous lattice simulations of the Roper channel, although they should inevitably appear as eigenstates in dynamical lattice QCD. In addition to being important representatives of the $N\pi$ and $N\pi\pi$ continuum, their energies and number in principle provide phase shifts for the scattering of nucleons and pions. These, in turn, provide information on the Roper resonance that resides in this channel. In the approximation when $N\pi$ is decoupled from other channels the $N\pi$ phase shift and the scattering matrix are directly related to eigenenergies via the Lüscher method [20,21]. The determination of the scattering matrix for coupled two-hadron channels has been proposed in [35,36] and was recently extracted from a lattice QCD simulation [37,38] for other cases. The presence of the three-particle decay mode $N\pi\pi$ in the Roper channel, however, poses a significant challenge to the rigorous treatment, as the scattering matrix for three-hadron decay has not been extracted from the lattice yet, although impressive progress on the analytic side has been made [39].

The purpose of the present paper is to determine the complete discrete spectrum for the interacting system with $J^P = 1/2^+$, including multi-hadron eigenstates. Zero total momentum is considered since parity is a good quantum number in this case. In addition to qqq interpolating fields, we incorporate for the first time $N\pi$ in p-wave in order to address their scattering. The $N\sigma$ in s-wave is also employed to account for $N(\pi\pi)^{I=0}_{s\text{-wave}}$. We aim at the energy region below 1.65 GeV, where the Roper resonance is observed in experiment. In absence of meson-meson and meson-baryon interactions one expects eigenstates dominated by $N(0)$, $N(0)\pi(0)\pi(0)$, $N(0)\sigma(0)$ and $N(1)\pi(-1)$, in our $N_f = 2+1$ dynamical simulation for $m_\pi \simeq 156$ MeV and $L \simeq 2.9$ fm. The momenta in units of $2\pi/L$ are given in parentheses. N and π in $N\pi$ need at least momentum $2\pi/L$ to form the p-wave. The PACS-CS configurations [40] have favorable parameters since the noninteracting energy $\sqrt{m_\pi^2 + (2\pi/L)^2} + \sqrt{m_N^2 + (2\pi/L)^2} \simeq 1.5$ GeV of $N(1)\pi(-1)$ falls in the Roper region. The number of observed eigenstates and their energies will lead to certain implications concerning the Roper resonance.

In the approximation of elastic $N\pi$ scattering, decoupled from $N\pi\pi$, the experimentally measured $N\pi$ phase shift predicts four eigenstates below 1.65 GeV, as argued in Sec. IV A and Fig. 7. Further analytic guidance for this channel was recently presented in [8], where the expected discrete lattice spectrum (for our L and m_π) was calculated using a Hamiltonian effective field theory (HEFT) approach for three hypotheses concerning the Roper state (Fig. 8). All scenarios involve channels $N\pi/N\sigma/\Delta\pi$ (assuming stable σ and Δ) and are apt to reproduce the experimental $N\pi$ phase shifts. The scenario which involves also a bare Roper qqq core predicts four eigenstates in the region $E < 1.7$ GeV of our interest, while the scenario without Roper qqq core predicts three eigenstates [8].[2] The Roper resonance in the second case is dynamically generated purely from the $N\pi/N\sigma/\Delta\pi$ channels, possibly accompanied by the ground state nucleon qqq core.

[1]The χQCD collaboration [30] recently verified that SEB and the variational approach with wide smeared sources ($r \simeq 0.8$ fm) lead to compatible $E \simeq 1.9$ GeV for Wilson-clover fermions and $m_\pi \simeq 400$ MeV.

[2]This numbering omits the $\Delta(1)\pi(-1)$ and $N(1)\sigma(-1)$ eigenstates that are near 1.7 GeV; these are not expected to be found in our study since the corresponding interpolators are not included. Our notation implies projection of all operators to $J^P = \frac{1}{2}^+$.

As already mentioned, our aim is to establish the expected low-lying multiparticle states in the positive-parity nucleon channel. This has been already accomplished in the negative-parity channel, where $N\pi$ scattering in s-wave was simulated in [41]. An exploratory study [42] was done in a moving frame, where both parities contribute to the same irreducible representation. The only lattice simulation in the positive-parity channel that included (local) $qqqq\bar{q}$ interpolators in addition to qqq was recently presented in [19]. No energy levels were found between m_N and $\simeq$2 GeV for $m_\pi \simeq 411$ MeV. The levels related to $N(1)\pi(-1)$ and $N(0)\sigma(0)$ were not observed, although they are expected below 2 GeV according to [8]. This is possibly due to the local nature of the employed $qqqq\bar{q}$ interpolators [19], which seem to couple too weakly to multi-hadron states in practice.

This paper is organized as follows. Section II presents the ensemble, methodology, interpolators and other technical details to determine the eigenenergies. The resulting eigenenergies and overlaps are presented in Sec. III, together with a discussion on the extraction of the $N\pi$ phase shift. The physics implications are drawn in Sec. IV and an outlook is given in the conclusions.

II. LATTICE SETUP

A. Gauge configurations

We perform a dynamical calculation on 197 gauge configurations generated by the PACS-CS collaboration with $N_f = 2 + 1$, lattice spacing $a = 0.0907(13)$ fm, lattice extension $V = 32^3 \times 64$, physical volume $L^3 \simeq (2.9)$ fm^3 and $\kappa_{u/d} = 0.13781$ [40]. The quark masses, $m_u = m_d$, are nearly physical and correspond to $m_\pi = 156(7)(2)$ MeV as estimated by PACS-CS [40]. Our own estimate leads to somewhat larger m_π as detailed below (we still refer to it as an ensemble with $m_\pi \simeq 156$ MeV). The quarks are non-perturbatively improved Wilson-clover fermions, which do not respect exact chiral symmetry (i.e., the Ginsparg-Wilson relation [43]) at nonzero lattice spacing a. Most of the previous simulations of the Roper channel also employed Wilson-clover fermions, for example [23,24,26–28].

Closer inspection of this ensemble reveals that there are a few configurations responsible for a strong fluctuation of the pion mass, which is listed in Table I. Removing one or four of the "bad" configurations changes the pion mass by more than two standard deviations. The configuration-set "all" indicates the full set of 197 gauge configurations, while "all-1" ("all-4") indicates a subset with 196 (193) configurations where one (four) configuration(s) leading to the strong fluctuations in m_π are removed.[3]

[3]In the set RC32x64_B1900Kud01378100Ks01364000 C1715 configuration jM000260 is removed in "all-1," while jM000260, hM001460, jM000840 and jM000860 are removed in "all-4."

TABLE I. The single hadron masses obtained for the full ("all") set of configurations and for the sets with one ("all-1") or four ("all-4") configurations omitted. Interpolators, fit type and fit range are like in Table II. As discussed in the text our final results are based on set "all-4."

Configuration set	m_π [MeV]	m_N [MeV]
all	153.9 ± 4.1	951 ± 19
all-1	163.9 ± 2.4	965 ± 13
all-4	164.4 ± 2.1	969 ± 12

We tested these three configuration sets for a variety of hadron energies, and we find that only m_π varies outside the statistical error, while variations of masses for other hadrons (mesons with light and/or heavy quarks and nucleon) are smaller than the statistical errors. This also applies for the nucleon mass listed in Table I. The energies of the pions and other hadrons with nonzero momentum also do not vary significantly with this choice.

The Roper resonance is known to be challenging as far as statistical errors are concerned, especially for nearly physical quark masses. The error on the masses and energies is somewhat bigger for the full set than on the reduced sets in some cases, for example m_π and m_N in Table I. Throughout this paper, we will present results for the reduced configuration set "all-4," unless specified differently. The final spectrum was studied for all three configuration sets, and we arrive at the same conclusions for all of them.

B. Determining eigenenergies

We aim to determine the eigenenergies in the Roper channel, and we will need also the energies of a single π or N. Lattice computation of eigenenergies E_n proceeds by calculating the correlation matrix $C(t)$ for a set of interpolating fields $O_i(\bar{O}_i)$ that annihilate (create) the physics system of interest,

$$\begin{aligned} C_{ij}(t) &= \langle \Omega | O_i(t + t_{\mathrm{src}}) \bar{O}_j(t_{\mathrm{src}}) | \Omega \rangle \\ &= \sum_n \langle \Omega | O_i | n \rangle \mathrm{e}^{-E_n t} \langle n | \bar{O}_j | \Omega \rangle \\ &= \sum_n Z_i^n Z_j^{n*} \mathrm{e}^{-E_n t}, \end{aligned} \tag{1}$$

with overlaps $Z_i^n = \langle \Omega | O_i | n \rangle$. All our results are averaged over all the source time slices $t_{\mathrm{src}} = 1, \ldots, 64$.

The E_n and Z_j^n are extracted from $C(t)$ via the generalized eigenvalue method [44–47]

$$C(t) u^{(n)}(t) = \lambda^{(n)}(t) C(t_0) u^{(n)}(t), \quad \lambda^{(n)}(t) \propto \mathrm{e}^{-E_n t} \tag{2}$$

and we apply $t_0 = 2$ for all cases except for the single pion correlation where we choose $t_0 = 3$. The large-time behavior of the eigenvalue $\lambda^{(n)}(t)$ provides E_n, where specific fit forms will be mentioned case by case. The

$$Z_j^n(t) = e^{E_n t/2} C_{jk}(t) u_k^{(n)}(t) / |C(t)^{\frac{1}{2}} u^{(n)}(t)| \qquad (3)$$

give the overlap factors in the plateau region.

For fitting E_n from $\lambda^{(n)}(t)$ we usually employ a sum of two exponentials, where the second exponential helps to parametrize the residual contamination from higher energy states at small t values. For the single pion ground state we have a large range of t-values to fit and there we combine $\cosh[E_n(t - N_T/2)]$ also with such an exponential. Correlated fits are used throughout. Single-elimination jackknife is used for statistical analysis.

C. Quark smearing width and distillation

The interpolating fields are built from the quark fields and we employ these with two smearing widths illustrated in Fig. 1. Linear combinations of operators with different smearing widths provide more freedom to form the eigenstates with nodes in the radial wave function. This is favorable for the Roper resonance [22,28,32], which is a radial excitation within a quark model.

Quark smearing is implemented using the so-called distillation method [48]. The method is versatile and enables us to compute all necessary Wick contractions, including terms with quark annihilation. This is made possible by precalculating the quark propagation from specific quark sources. The sources are the lowest $k = 1, \ldots, N_v$ eigenvectors $v^k_{\mathbf{x}c}$ of the spatial lattice Laplacian and c is the color index. Smeared quarks are provided by $q^c(\mathbf{x}) \equiv \Box_{\mathbf{x}'c',\mathbf{x}c} q^{c'}_{\text{point}}(\mathbf{x}')$ [48] with the smearing operator $\Box_{\mathbf{x}'c',\mathbf{x}c} = \sum_{k=1}^{N_v} v^k_{\mathbf{x}'c'} v^{k\dagger}_{\mathbf{x}c}$. Different N_v lead to different effective smearing widths.

In previous work we used stochastic distillation [49] on this ensemble, which is less costly but renders noisier results. For the present project we implemented the distillation[4] with narrower (n) smearing $N_v = 48$ and wider (w) smearing $N_v = 24$, illustrated in Fig. 1. Two smearings are employed to enhance freedom in forming the eigenstates with nodes. Most of the interpolators and results below are based on narrower smearing which gives better signals in practice, although both widths are not very different. The details of our implementation of the distillation method are collected in [50] for another ensemble.

D. Interpolators and energies of π and N

Single particle energies are needed to determine reference energies of the noninteracting (i.e., disregarding interaction between the mesons and baryons) system, and also to examine phase shifts (see Sec. III B). The following π and N annihilation interpolators are used to extract energies of the single hadrons with momenta $\mathbf{n}2\pi/L$

[4]This is sometimes referred to as the full distillation.

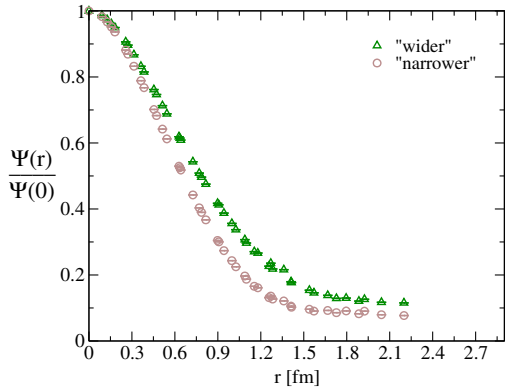

FIG. 1. The profile $\Psi(r)$ of the "narrower" ($N_v = 48$) and the "wider" ($N_v = 24$) smeared quark, where $\Psi(r) = \sum_{\mathbf{x},t} \sqrt{\mathrm{Tr}_c[\Box_{\mathbf{x},\mathbf{x}+\mathbf{r}}(t)\Box_{\mathbf{x},\mathbf{x}+\mathbf{r}}(t)]}$.

(these are also used as building blocks for interpolators in the Roper channel):

$$\pi^+(\mathbf{n}) = \sum_{\mathbf{x}} \bar{d}(\mathbf{x},t)\gamma_5 u(\mathbf{x},t) e^{i\mathbf{x}\cdot\mathbf{n}\frac{2\pi}{L}}$$
$$\pi^0(\mathbf{n}) = \frac{1}{\sqrt{2}} \sum_{\mathbf{x}} [\bar{d}(\mathbf{x},t)\gamma_5 d(\mathbf{x},t) - \bar{u}(\mathbf{x},t)\gamma_5 u(\mathbf{x},t)] e^{i\mathbf{x}\cdot\mathbf{n}\frac{2\pi}{L}} \qquad (4)$$

and

$$N^i_{m_s=1/2}(\mathbf{n}) = \mathcal{N}^i_{\mu=1}(\mathbf{n}), \qquad N^i_{m_s=-1/2}(\mathbf{n}) = \mathcal{N}^i_{\mu=2}(\mathbf{n})$$
$$\mathcal{N}^i_\mu(\mathbf{n}) = \sum_{\mathbf{x}} \epsilon_{abc} [u^{aT}(\mathbf{x},t)\Gamma^i_2 d^b(\mathbf{x},t)] \times [\Gamma^i_1 q^c(\mathbf{x},t)]_\mu e^{i\mathbf{x}\cdot\mathbf{n}\frac{2\pi}{L}}$$
$$i = 1,2,3: \ (\Gamma^i_1, \Gamma^i_2) = (\mathbf{1}, C\gamma_5), (\gamma_5, C), (i\mathbf{1}, C\gamma_t\gamma_4). \qquad (5)$$

Three standard choices for $\Gamma_{1,2}$ are used. The third quark is $q = u$ for the proton and $q = d$ for the neutron. Equation (5) is in Dirac basis and the upper two components $\mathcal{N}_{\mu=1,2}$ of the Dirac four spinor $\mathcal{N}_\mu$ are the ones with positive parity at zero momentum. The spin component m_s in N_{m_s} is a good quantum number for $\mathbf{p} = 0$ or $\mathbf{p} \propto e_z$, which is employed to determine energies in Table II. It is not a good quantum number for general $\mathbf{p}$ and it denotes the spin component m_s of the corresponding field at rest. The "noncanonical" fields $N_{m_s}(\mathbf{n})$ (5) built only from upper components have the desired transformation properties under rotation R and inversion I, which are necessary to build two-hadron operators [51]:

$$RN_{m_s}(\mathbf{n})R^\dagger = \sum_{m'_s} D^{1/2}_{m_s m'_s}(R^\dagger) N_{m'_s}(R\mathbf{n}),$$
$$R\pi(\mathbf{n})R^\dagger = \pi(R\mathbf{n}) \qquad IN_{m_s}(\mathbf{n})I = N_{m_s}(-\mathbf{n}),$$
$$I\pi(\mathbf{n})I = -\pi(-\mathbf{n}). \qquad (6)$$

TABLE II. The energies of single hadrons π and N for two relevant momenta, based on configuration set "all-4." Energies in GeV are obtained by multiplying with $1/a \simeq 2.17$ GeV.

Hadron	$\mathbf{n} = \frac{\mathbf{p}L}{2\pi}$	Interpolator	Fit range	Fit type	χ^2/dof	Ea (lat)	$E^c a = a\sqrt{m^2 + \mathbf{p}^2}$
π	(0, 0, 0)	π	8–18	cosh + exp, c	0.99	0.07558 ± 0.00098	
π	(0, 0, 1)	π	6–20	2 exp, c	1.91	0.2049 ± 0.0023	0.2104
N	(0, 0, 0)	$N_n^{1,3}$	4–12	2 exp, c	0.39	0.4455 ± 0.0056	
N	(0, 0, 1)	$N_n^{1,3}$	4–12	2 exp, c	0.54	0.4920 ± 0.0072	0.4864

Interpolators with narrower quark sources are used for the determination of the masses and energies of π and N. Those are collected in Table II, where they are compared to energies E^c expected in the continuum limit $a \to 0$.

E. Interpolating fields for the Roper channel

Our central task is to calculate the energies of the eigenstates E_n with $J^P = 1/2^+$ and total momentum zero, including multiparticle states. We want to cover the energy range up to approximately 1.65 GeV, which is relevant for the Roper region. The operators with these quantum numbers have to be carefully constructed. Although qqq interpolators in principle couple also to multi-hadron intermediate states in dynamical QCD, the multi-hadron eigenstates are often not established in practice unless the multi-hadron interpolators are also employed in the correlation matrix.

We apply ten interpolators $O_{i=1,\ldots,10}$ with $P = +$, $S = 1/2$, $(I, I_3) = (1/2, 1/2)$ and total momentum zero [51] (P and m_s are good continuum quantum numbers in this case). For $m_s = 1/2$, we have

$$\begin{aligned}
O_{1,2}^{N\pi} &= -\sqrt{\frac{1}{3}}[p_{-\frac{1}{2}}^{1,2}(-e_x)\pi^0(e_x) - p_{-\frac{1}{2}}^{1,2}(e_x)\pi^0(-e_x) \\
&\quad - ip_{-\frac{1}{2}}^{1,2}(-e_y)\pi^0(e_y) + ip_{-\frac{1}{2}}^{1,2}(e_y)\pi^0(-e_y) \\
&\quad + p_{\frac{1}{2}}^{1,2}(-e_z)\pi^0(e_z) - p_{\frac{1}{2}}^{1,2}(e_z)\pi^0(-e_z)] \\
&\quad + \sqrt{\frac{2}{3}}[\{p \to n, \pi^0 \to \pi^+\}] \quad \text{[narrower]} \\
O_{3,4,5}^{N_w} &= p_{\frac{1}{2}}^{1,2,3}(0) \quad \text{[wider]} \\
O_{6,7,8}^{N_n} &= p_{\frac{1}{2}}^{1,2,3}(0) \quad \text{[narrower]} \\
O_{9,10}^{N\sigma} &= p_{\frac{1}{2}}^{1,2}(0)\sigma(0) \quad \text{[narrower]},
\end{aligned} \tag{7}$$

where these are the annihilation fields and

$$\sigma(0) = \frac{1}{\sqrt{2}}\sum_{\mathbf{x}}[\bar{u}(\mathbf{x}, t)u(\mathbf{x}, t) + \bar{d}(\mathbf{x}, t)d(\mathbf{x}, t)]. \tag{8}$$

The momenta of fields in units of $2\pi/L$ are given in parentheses with e_x, e_y, and e_z denoting the unit vectors in x, y, and z directions, while the lower index on $N = p, n$ is m_s. All quarks have the same smearing width (narrower or wider in Fig. 1) within one interpolator. The $O^{N\pi}$ was constructed in [51], while factors with square root are Clebsch-Gordan coefficients related to isospin. For $m_s = -1/2$, $p_{1/2}$ and $n_{1/2}$ gets replaced by $p_{-1/2}$ and $n_{-1/2}$ in O_{3-10}, while $O_{1,2}$ becomes [51]

$$\begin{aligned}
O_{1,2}^{N\pi} &= -\sqrt{\frac{1}{3}}[p_{\frac{1}{2}}^{1,2}(-e_x)\pi^0(e_x) - p_{\frac{1}{2}}^{1,2}(e_x)\pi^0(-e_x) \\
&\quad + ip_{\frac{1}{2}}^{1,2}(-e_y)\pi^0(e_y) - ip_{\frac{1}{2}}^{1,2}(e_y)\pi^0(-e_y) \\
&\quad - p_{-\frac{1}{2}}^{1,2}(-e_z)\pi^0(e_z) + p_{-\frac{1}{2}}^{1,2}(e_z)\pi^0(-e_z)] \\
&\quad + \sqrt{\frac{2}{3}}[\{p \to n, \pi^0 \to \pi^+\}] \quad \text{[narrower]}.
\end{aligned} \tag{9}$$

The basis (7) contains conventional qqq fields as well as the most relevant multi-hadron components. The noninteracting levels below 1.65 GeV are $N(0)$, $N(1)\pi(-1)$, $N(0)\pi(0)\pi(0)$ and, assuming zero width approximation, $N(0)\sigma(0)$. The $N(2)\pi(-2)$, $N(1)\pi(-1)\pi(0)$ and others are at higher energies. Here $O^{N\pi}$ corresponds to $N(1)\pi(-1)$ in p-wave [51]. Our notation implies projection to $J^P = \frac{1}{2}^+$ for all operators [e.g., $N(1)\sigma(-1)$ actually refers to $\sum_{\mu=1}^{3} N(e_\mu)\sigma(-e_\mu)$]. Interpolators $N(n)\pi(-n)$ with $n \geq 2$ are not incorporated, so we do not expect to find those in the spectrum. We implement only one type of σ interpolator (8) in $O^{N\sigma}$ and we expect that this represents a possible superposition of $N\pi\pi$ and $N\sigma$.[5]

On the discrete lattice the continuum rotation symmetry group is reduced to the discrete lattice double-cover group O_h^2. The states with the continuum quantum number $J^P = 1/2^+$ transform according to the G_1^+ irreducible representation on the lattice. All operators (7) indeed transform according to G_1^+,

$$\begin{aligned}
RO_i^{m_s}(0)R^\dagger &= \sum_{m_s'} D_{m_s m_s'}^{1/2}(R^\dagger)O_i^{m_s'}(0), \\
IO_i^{m_s}(0)I &= O_i^{m_s}(0),
\end{aligned} \tag{10}$$

[5]The σ channel itself was recently simulated with a number of interpolators in [52].

TABLE III. Number of Wick contractions involved in computing correlation functions between interpolators in Eq. (7).

$O_i \backslash O_j$	O^N	$O^{N\pi}$	$O^{N\sigma}$
O^N	2	4	7
$O^{N\pi}$	4	19	19
$O^{N\sigma}$	7	19	33

as can be checked by using the transformations of individual fields N, π, σ [Eqs. (4), (5), and (8)]. The $N\pi$ operator with such transformation properties was constructed using the projection, partial-wave and helicity methods [51], all leading to $O^{N\pi}_{1,2}$ in Eqs. (7) and (9). The partial-wave method indicates that it describes $N\pi$ in p-wave.

We restrict our calculations to zero total momentum since parity is a good quantum number in this case. The positive parity states with $J = 1/2$ as well as $J \geq 7/2$ appear in the relevant irreducible representation G_1^+ of O_h^2. The observed baryons with $J \geq 7/2$ lie above 1.9 GeV, therefore this does not present a complication for the energy region of our interest. We do not consider the system with nonzero total momenta since $1/2^+$ as well as $1/2^-$ (and others) appear in the same irreducible representation [53], which would be a significant complication especially due to the negative parity states $N(1535)$ and $N(1650)$.

F. Wick contractions for the Roper channel

The 10×10 correlation function $C_{ij}(t)$ (1) for the Roper channel is obtained after evaluating the Wick contractions for any pair of source $\bar{O}_j$ and sink O_i. The number of Wick contractions involved in computing the correlation functions between our interpolators [Eqs. (7)] is tabulated in Table III.

The $O^N \leftrightarrow O^N$ contractions have been widely used in the past. The 19 Wick contractions $O^{N\pi} \leftrightarrow O^{N\pi}$ and four Wick contractions $O^N \leftrightarrow O^{N\pi}$ are the same as in the Appendix of [41], where the negative-parity channel was studied. The inclusion of $O^{N\sigma}$ introduces additional $2 \cdot 7 + 2 \cdot 19 + 33$ Wick contractions, while the inclusion of three hadron interpolators like $N\pi\pi$ would require many more. We evaluate all necessary contractions in Table III using the distillation method [48] discussed in Sec. II C.

Appendix V illustrates how to handle the spin components in evaluating $C(t)$, where one example of the Wick contraction $\langle\Omega|O^{N\pi}\bar{O}^N|\Omega\rangle$ is considered.

III. RESULTS

A. Energies and overlaps

Our main result is the energies of the eigenstates in the $J^P = 1/2^+$ channel, shown in Fig. 2(a). These are based on the 5×5 correlation matrix (1) for the subset of interpolators (7)

$$\text{complete interpolator set}: \quad O_1^{N\pi}, \quad O_3^{N_n}, \quad O_{6,8}^{N_w}, \quad O_9^{N\sigma}, \tag{11}$$

which we refer to as the "complete set" since it contains all types of interpolators. Adding other interpolators to this basis, notably $O_{2,4,7,10}$, which include the $N^{i=2}$ interpolator,[6] makes the eigenenergies noisier. The eigenenergies E_n are obtained from the fits of the eigenvalues $\lambda^{(n)}(t)$ (2), with fit details in Table IV. The horizontal dashed lines represent the energies of the expected multihadron states $m_N + 2m_\pi$ and $E_{N(1)} + E_{\pi(-1)}$ in the noninteracting limit (the individual hadron energies measured on our lattice and given in Table II are used for this purpose throughout this work). The study of this channel with almost physical pion mass is challenging as far as statistical errors are concerned. This can be seen from the effective energies in Fig. 3 which give eigenenergies in the plateau region.

TABLE IV. The final energies E_n of eigenstates in the Roper channel, which correspond to Fig. 2(a) and effective masses in Fig. 3. They are obtained from correlated fits based on the complete interpolator set [Eq. (11)] and configuration set "all-4." Energies in GeV can be obtained by multiplying with $1/a \simeq 2.17$ GeV.

Eigenstate n	Fit range	Fit type	χ^2/dof	Ea
1	4–12	2 exp, c	0.50	0.4427 ± 0.0055
2	4–12	2 exp, c	1.04	0.6196 ± 0.0266
3	4–10	2 exp, c	0.88	0.6873 ± 0.0195
4	4–7	1 exp, c	0.32	0.9527 ± 0.0338

The ground state ($n = 1$) in Fig. 2(a) represents the nucleon. The first-excited eigenstate ($n = 2$) lies near $m_N + 2m_\pi$ and appears to be close to $N(0)\pi(0)\pi(0)$ in the noninteracting limit. The next eigenstate $n = 3$ lies near the noninteracting energy $E_{N(1)} + E_{\pi(-1)}$. It dominantly couples to $O^{N\pi}$ and we relate it to $N(1)\pi(-1)$ in the noninteracting limit. Further support in favor of this identification for levels $n = 2$, 3 will be given in the discussion of Figs. 4 and 5. The most striking feature of the spectrum is that there are only three eigenstates below 1.65 GeV, while the other eigenstates appear at higher energy.

The overlaps of these eigenstates with various operators are presented in Fig. 2(b). The nucleon ground state $n = 1$ couples well with all interpolators that contain N^1. The operator $O^{N\pi}$ couples well with eigenstate $n = 3$, which

[6]It has been observed already earlier, e.g. [54], that this interpolator shows no plateau behavior in the effective energy.

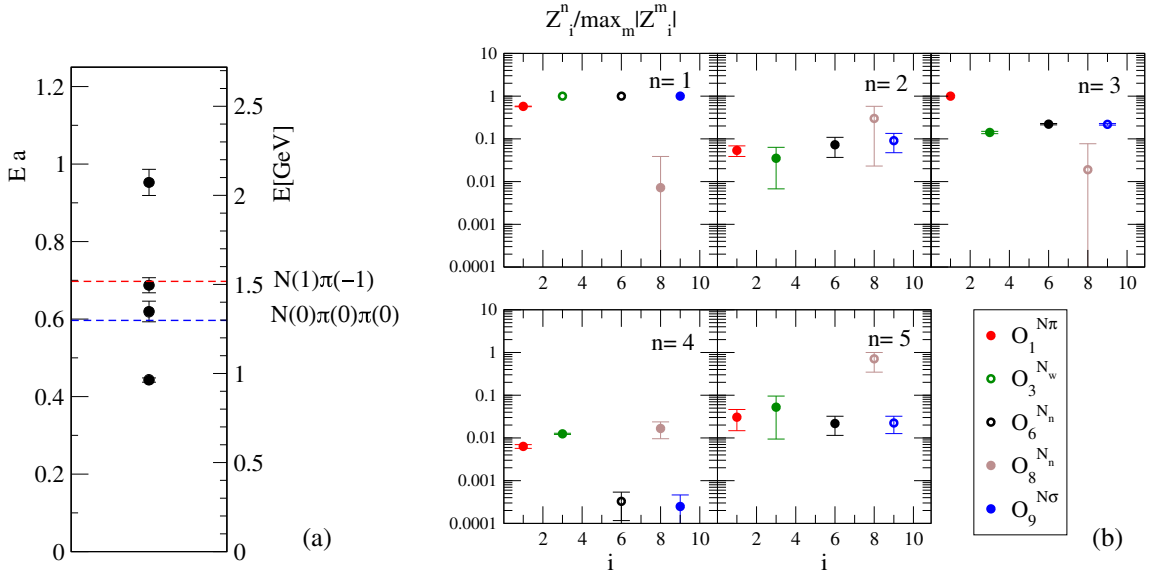

FIG. 2. The eigenenergies E_n (a) and normalized overlaps $Z_i^n = \langle\Omega|O_i|n\rangle$ (b), which result from correlation matrix (1) based on the complete interpolator set (11). (a) The energies E_n from lowest ($n = 1$) to highest ($n = 4$). The horizontal dashed lines represent the energies $m_N + 2m_\pi$ and $E_{N(1)} + E_{\pi(-1)}$ of the expected multi-hadron states in the noninteracting limit. (b) The ratios of overlaps Z_i^n with respect to the largest among $|Z_i^{m=1,\ldots,5}|$; these ratios are independent on the normalization of O_i. The full and empty symbols correspond to the positive and negative Z_i^n, respectively (Z_i^n are almost real). Configuration set "all-4" is used.

gives further support that this state is related to $N(1)\pi(-1)$. The operator $O^{N\sigma}$ couples best with the nucleon ground state, which is not surprising due to the presence of the Wick contraction where the isosinglet σ (8) annihilates and the remaining N^1 couples to the nucleon. Interestingly, the $O^{N\sigma}$ has similar couplings to the eigenstates $n = 2$ and $n = 3$, which are related to $N(0)\pi(0)\pi(0)$ and $N(1)\pi(-1)$ in the noninteracting limit. One would expect $|\langle\Omega|O^{N\sigma}|n = 2\rangle| \gg |\langle\Omega|O^{N\sigma}|n = 3\rangle|$ if the channel $N\pi$ were decoupled from $N\sigma/N\pi\pi$. Our overlaps $Z_{i=9}^{n=2,3}$ suggest that the channels are significantly coupled. The scenario where the coupled-channel scattering might be crucial for the Roper resonance will discussed in Sec. IV.

The features of the spectrum for various choices of the interpolator basis are investigated in Fig. 4. The complete set (11) with all types of interpolators is highlighted as choice 1. If the operator $O^{N\pi}$ is removed (choice 3) the eigenstate with energy $\simeq E_{N(1)} + E_{\pi(1)}$ disappears, so the $N\pi$ Fock component is important for this eigenstate. The eigenstate with energy $\simeq m_N + 2m_\pi$ disappears if $O^{N\sigma}$ is removed (choice 4), which suggests that this eigenstate is dominated by $N(0)\pi(0)\pi(0)$, possibly mixed with $N(0)\sigma(0)$. Any interpolator individually renders the nucleon as a ground state (choices 5, 6, and 7).

All previous lattice simulations, except for [19], used just qqq interpolators. This is represented by choice 5, which renders the nucleon, while the next state is above 1.65 GeV; this result is in agreement with most of the previous lattice results based on qqq operators, discussed in the Introduction. No interpolator basis renders more than three eigenstates below 1.65 GeV.

The most striking feature of the spectra in Figs. 2 and 4 is the absence of any additional eigenstate in the energy region where the Roper resonance resides in experiment. The eigenstates $n = 2$, 3 lie in this energy region, but two eigenstates related to $N(0)\pi(0)\pi(0)$ and $N(1)\pi(-1)$ are inevitably expected there in dynamical QCD, even in the absence of the interactions between hadrons.

A further indication that eigenstate $n = 2$ is dominated by $N(0)\pi(0)\pi(0)$ is presented in Fig. 5, where the spectrum from all configurations is compared to the spectrum based on configuration sets "all-4" (shown in other figures) and "all-1." The horizontal dashed lines indicate noninteracting energies obtained from the corresponding sets. Only the central values of E_2 and $m_N + 2m_\pi$ visibly depend on the configuration set. The variation of $m_N + 2m_\pi$ is due to the variations of m_π pointed out in Sec. II A. The eigenstate $n = 2$ appears to track the threshold $m_N + 2m_\pi$, which suggests that its Fock component $N(0)\pi(0)\pi(0)$ is important. Note that the full configuration set gives larger statistical errors, as illustrated via effective masses in Fig. 9 of Appendix B.

B. Scattering phase shift

In order to discuss the $N\pi$ phase shift, we consider the elastic approximation where $N\pi$ scattering is decoupled from the $N\pi\pi$ channel. In this case, the $N\pi$ phase shift δ can

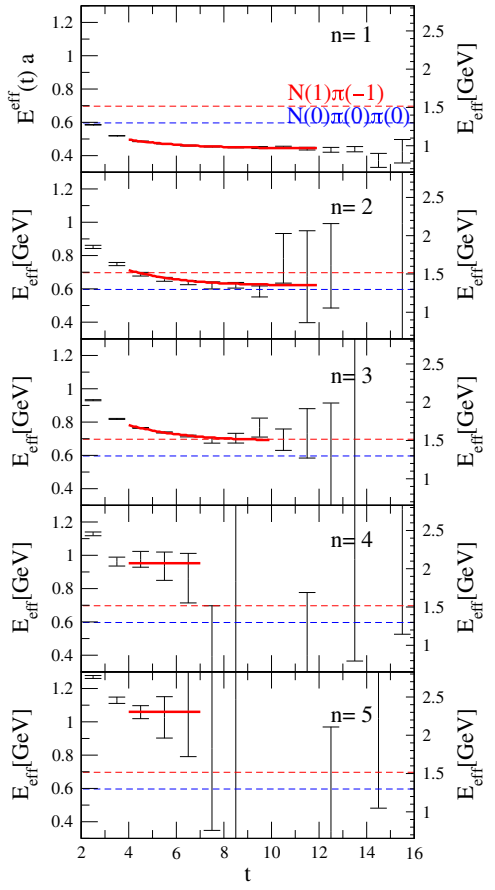

FIG. 3. The effective energies $E_n^{\mathrm{eff}}(t) = \log[\lambda^{(n)}(t)/\lambda^{(n)}(t+1)] \to E_n$ of eigenvalues $\lambda^{(n)}$. These correspond to the energies of eigenstates E_n in Fig. 2(a) and Table IV. It is based on the complete interpolator set (11) and configuration set "all-4." The fits of $\lambda^{(n)}(t)$ that render E_n are also presented. Noninteracting energies of $N(0)\pi(0)\pi(0)$ and $N(1)\pi(-1)$ are shown with dashed lines.

be determined from the eigenenergy E of the interacting state $N\pi$ via Lüscher's relation [20,21]

$$\delta(p) = \mathrm{atan}\left[\frac{\sqrt{\pi}pL}{2Z_{00}(1;(\frac{pL}{2\pi})^2)}\right],$$
$$E = E_{N(p)} + E_{\pi(p)}, \tag{12}$$

where $E_{H(p)} = \sqrt{m_H^2 + p^2}$ applies in the continuum limit. The eigenenergy E (E_3 from basis $O^{N\pi,N,N\sigma}$ or E_2 from $O^{N\pi,N}$) has sizable error for this ensemble with close-to-physical pion mass. It lies close to the noninteracting energy $E_{N(1)} + E_{\pi(1)}$, as can be seen in Figs. 2, 3 and 9. We find that the resulting energy shift $\Delta E = E - E_{N(1)} - E_{\pi(1)}$ is consistent with zero (modulo π) within the errors. This implies that the phase shift δ is zero within a large statistical error.

We verified this using a number of choices to extract ΔE and δ. The interpolator set $O^{N\pi,N}$ (rightmost column of Fig. 9) that imitates the elastic $N\pi$ scattering served as a main choice, while it was compared to other sets also. Correlated and uncorrelated fits of E as well as $E_{N(1)} + E_{\pi(1)}$ were explored for various fit ranges. Further choices of dispersion relations $E_\pi(p)$ and $E_N(p)$ that match lattice energies at $p = 0$, 1 in Table II (e.g., interpolation of E^2 linear in p^2) were investigated within the Lüscher analysis to arrive at same conclusions.

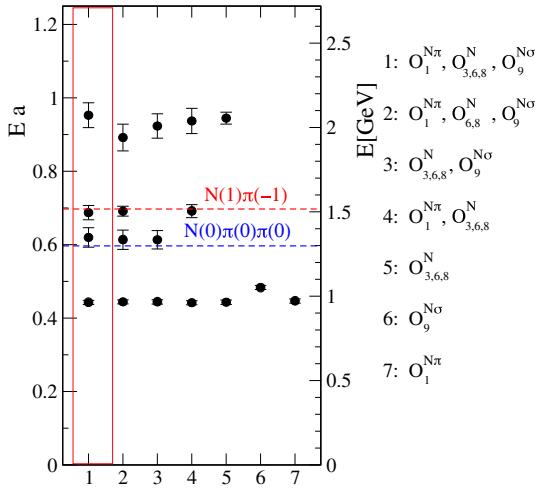

FIG. 4. The energies of eigenstates E_n for various choices of interpolator basis (7) used in correlation matrix [(1) and (2)]. The reference choice 1 representing the complete interpolator set $O_1^{N\pi}, O_3^{N_w}, O_{6,8}^{N_n}, O_9^{N\sigma}$ (11) is highlighted. One or more interpolators are removed for other choices. The horizontal lines present noninteracting energies of $N(0)\pi(0)\pi(0)$ and $N(1)\pi(-1)$. Results are based on configuration set "all-4."

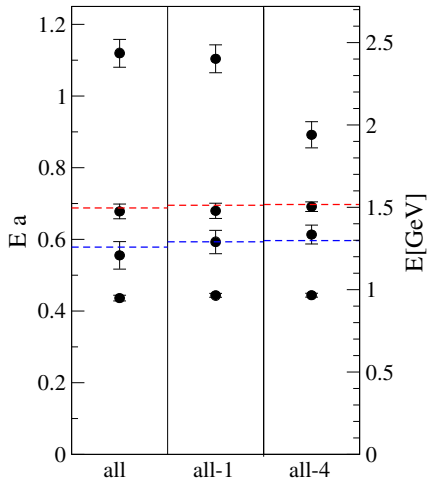

FIG. 5. The energies E_n are determined on all 197 configurations ("all"), on 196 configurations ("all-1"), and on 193 configurations ("all-4"), as described in Sec. II A. The values are based on the interpolator set $O_1^{N\pi}, O_{6,8}^{N_n}, O_9^{N\sigma}$ which gives smaller statistical errors than set (11) for "all" and "all-1." The horizontal lines present noninteracting energies of $N(0)\pi(0)\pi(0)$ and $N(1)\pi(-1)$ for the corresponding configuration sets.

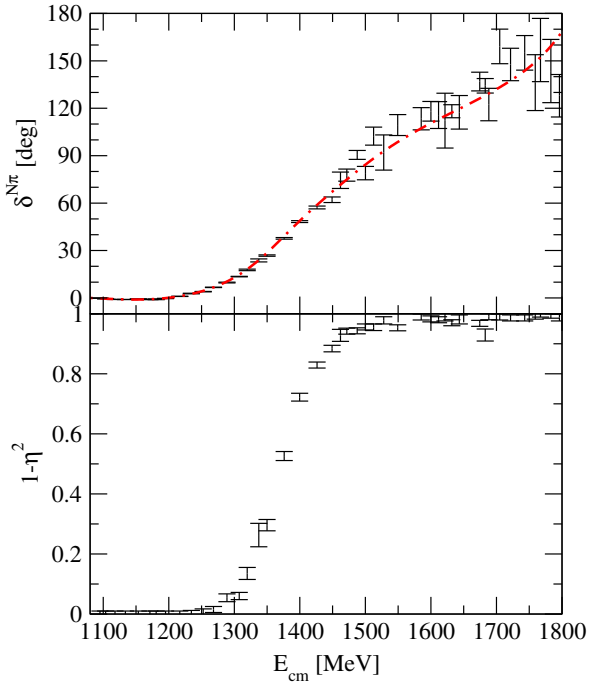

FIG. 6. The experimental phase shift δ and inelasticity $1-\eta^2$ as extracted by the GWU group [55] (solution WI08). The dot-dashed line is a smooth interpolation that is used in Sec. IV A.

IV. DISCUSSION AND INTERPRETATION

Here we discuss the implications of our results, in particular that only three eigenstates are found below 1.65 GeV. These appear to be associated with $N(0)$, $N(0)\pi(0)\pi(0)$ and $N(1)\pi(-1)$ in the noninteracting limit.

The experimental $N\pi$ scattering data for the amplitude $T=(\eta e^{2i\delta}-1)/(2i)$ for this (P_{11}) channel are shown in Fig. 6 [55].[7] The channel is complicated by the fact that $N\pi$ scattering is not elastic above the $N\pi\pi$ threshold and the inelasticity is sizable already in the energy region of the Roper resonance.

The presence of the $N\pi\pi$ channel prevents rigorous investigation on lattice at the moment. While the three-body channels have been treated analytically, see for example [39,57], the scattering parameters have not been determined in any channel within lattice QCD up to now. For this reason we consider implications for the lattice spectrum based on various simplified scenarios. By comparing our lattice spectra to the predictions of these scenarios, certain conclusions on the Roper resonance are drawn.

A. $N\pi$ scattering in elastic approximation

Let us examine what would be the lattice spectrum assuming experimental $N\pi$ phase shift in the approximation when $N\pi$ is decoupled from the $N\pi\pi$ channel. In addition we consider no interactions in the $N\pi\pi$ channel. The elastic phase shift δ in Fig. 6 allows to obtain the discrete energies E as a function of the spatial lattice size L via Lüscher's equation (12).

Figure 7(a) shows the noninteracting levels for $N(0)$ (black), $N(0)\pi(0)\pi(0)$ (blue), and $N(1)\pi(-1)$ (red). These are shifted by the interaction. Also plotted are the eigenstates (orange) in the interacting $N\pi$ channel derived from the experimental elastic phase shift with help of Eq. (12). The elastic scenario should therefore render four eigenstates below 1.65 GeV at our $L\simeq 2.9$ fm, indicated by the violet circles in Figs. 7(a) and 7(b). Three noninteracting levels[8] below 1.65 GeV turn into four interacting levels (violet circles) at $L\simeq 2.9$ fm. The Roper resonance phase shift passing $\pi/2$ is responsible for the extra level.

Our actual lattice data features only three eigenstates below 1.65 GeV, and no extra low-lying eigenstate is found. Comparison in Fig. 7(b) indicates that the lattice data is qualitatively different from the prediction of the resonating $N\pi$ phase shift for the low-lying Roper resonance, assuming it is decoupled from $N\pi\pi$.

B. Scenarios with coupled $N\pi - N\sigma - \Delta\pi$ scattering

Our analysis does not show the resonance related level. One reason could be that the Roper resonance is a truly coupled channel phenomenon and one has to include further interpolators like $\Delta\pi$, $N\rho$ and an explicit $N\pi\pi$ three hadron interpolator. The scattering of $N\pi - N\sigma - \Delta\pi$ in the Roper channel was studied recently using Hamiltonian effective field theory (HEFT) [8]. The σ and Δ were assumed to be stable under the strong decay, which is a (possibly serious) simplification. The free parameters were always fit to the experimental $N\pi$ phase shift and describe the data well. Three models were discussed:

(I) The three channels are coupled with a low-lying bare Roper operator of type qqq.
(II) No bare baryon; the $N\pi$ phase shift is reproduced solely via coupled channels.
(III) The three channels are coupled only to a bare nucleon.

The resulting Hamiltonian was considered in a finite volume leading to discrete eigenenergies for all three cases, plotted in Fig. 8 for our parameters $L=2.9$ fm and $m_\pi=156$ MeV [8].

In Fig. 8 we compare our lattice spectra with the prediction for energies of $J^P=1/2^+$ states in three scenarios. The stars mark the high-lying eigenstates $N(1)\sigma(-1)$, $\Delta(1)\pi(-1)$ and $N(2)\pi(-2)$ [8], which are not expected to be found in our study since we did not incorporate corresponding interpolators in (7). The squares denote predictions from the three scenarios that can be qualitatively compared with our lattice spectra.

[7]The experimental data comes from the GWU homepage [56].

[8]These are three intercepts of dashed curves with a vertical green line at $L=2.9$ fm.

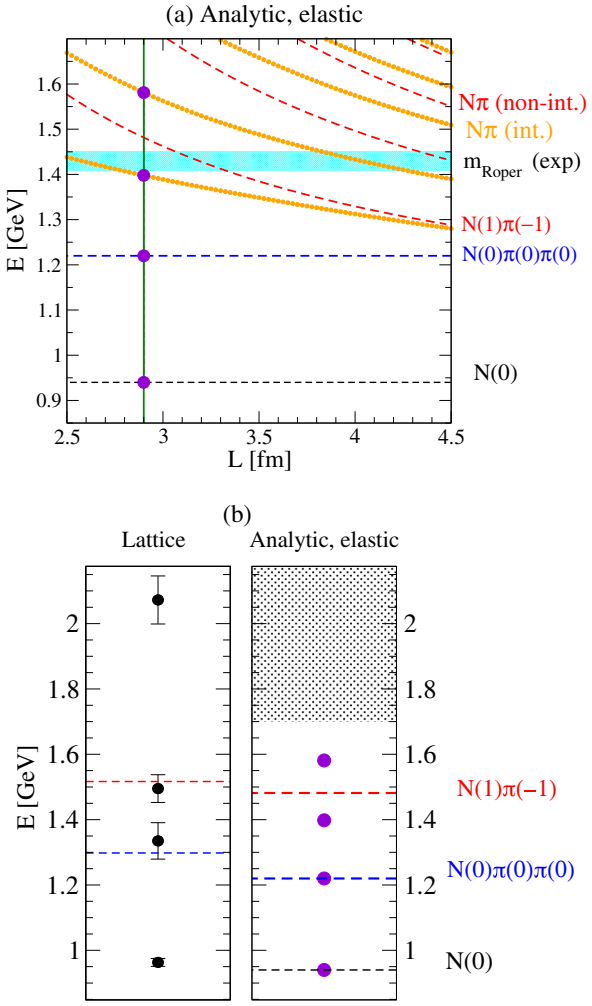

FIG. 7. (a) Analytic prediction for the eigenenergies E as a function of the lattice size L, according to (12). The $N\pi$ and $N\pi\pi$ are assumed to be decoupled, and $N\pi\pi$ is noninteracting. The curves show noninteracting $N\pi$ (red dashed), interacting $N\pi$ based on experimental phase shift [55] (orange dotted), $N\pi\pi$ threshold (blue dashed), proton mass (black), and Roper mass (cyan band). The experimental masses of hadrons are used. (b) Left: energy values from our simulation; right: the full violet circles show the analytic predictions for the energies at our $L = 2.9$ fm based on the experimental phase shift data and elastic approximation (same as violet circles in upper pane). We show only the energy region $E < 1.7$ GeV where we aim to extract the complete spectrum (there are additional multi-hadron states in the shaded region and we did not incorporate interpolator fields for those).

Our lattice levels below 1.7 GeV disagree with model I based on the bare Roper qqq core, but are consistent with II and (preferred) III with no bare Roper qqq core. In those scenarios the Roper resonance is dynamically generated from the $N\pi/N\sigma/\Delta\pi$ channels, coupled also to a bare nucleon core in case III. A preference for interpretations II and III was reached also in other phenomenological studies [6–9] and on the lattice [19], for example.

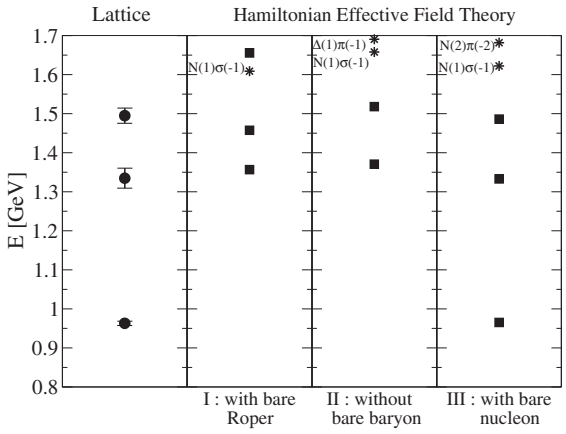

FIG. 8. Analytic predictions for the lattice spectra at $m_\pi = 156$ MeV and $L = 2.9$ fm from the Hamiltonian effective field theory. These are based on three scenarios concerning the Roper resonance [8]. Our lattice spectrum is shown with circles on the left. Qualitative comparison between the energies represented by squares and circles can be made, as discussed in the main text.

C. Hybrid baryon scenario

Several authors, for example [12,13], have proposed that the Roper resonance might be a hybrid baryon $qqqG$ with excited gluon field. This scenario predicts the longitudinal helicity amplitude $S_{1/2}$ to vanish [58], which is not supported by the measurement [59]. Our lattice simulation cannot provide any conclusion regarding this scenario since we have not incorporated interpolating fields of the hybrid type.

D. Other possibilities for absence of the resonance related level

Let us discuss other possible reasons for the missing resonance level in our results, beyond the coupled-channel interpretation offered above.

We could be missing the eigenstate because we might have missed important coupling operators. One such candidate might be a genuine pentaquark operator. A local five quark interpolator (with baryon-meson color structure) has been used by [19] who, however, also did not find a Roper signal. The local pentaquark operator with color structure $\epsilon_{abc}\bar{q}_a[qq]_b[qq]_c$ ($[qq]_c = \epsilon_{cde}q_cq_dq_e$) can be rewritten as a linear combination of local baryon-meson operators $BM = (\epsilon_{abc}q_aq_bq_c)(\bar{q}_eq_e)$ by using $\epsilon_{abc}\epsilon_{ade} = \delta_{bd}\delta_{ce} - \delta_{be}\delta_{cd}$. Furthermore, the local baryon-meson operators are linear combinations of $B(\mathbf{p})M(-\mathbf{p})$. Among various terms, the $N(1)\pi(-1)$ and $N(0)\sigma(0)$ are the essential ones for the explored energy region and those were incorporated in our basis (7). So, we expect that our simulation does incorporate the most essential operators in the linear combination representing the genuine localized pentaquark operator. It remains to be seen if structures with significantly separated diquark (such as proposed in [60] for P_c) could be also be probed by baryon-meson operators like (7).

It could also be that—contrary to our expectation—using operators with different quark smearing widths is not sufficient to scan the qqq radial excitations. One might have to expand the interpolator set to include nonlocal interpolators [26] so as to have good overlap with radial excitations with nontrivial nodal structures. There has been no study that involved use of such operators along with the baryon-meson operators and within the single hadron approach such operators do not produce low-lying levels in the Roper energy range [26].

Finally, our results are obtained using fermions that do not obey exact chiral symmetry at finite lattice spacing a, like in most of the previous simulations. It would be desirable to verify our results using fermions that respect chiral symmetry at finite a.

V. CONCLUSION AND OUTLOOK

We have determined the spectrum of the $J^P = 1/2^+$ and $I = 1/2$ channel below 1.65 GeV, where the Roper resonance appears in experiment. This lattice simulation has been performed on the PACS-CS ensemble with $N_f = 2 + 1$, $m_\pi \simeq 156$ MeV and $L = 2.9$ fm. Several interpolating fields of type qqq (N) and $qqqq\bar{q}$ ($N\sigma$ in s-wave and $N\pi$ in p-wave) were incorporated, and three eigenstates below 1.65 GeV are found. The energies, their overlaps to the interpolating fields and additional arguments presented in the paper indicate that these are related to the states that correspond to $N(0)$, $N(0)\pi(0)\pi(0)$ and $N(1)\pi(-1)$ in the noninteracting limit (momenta in units of $2\pi/L$ are given in parentheses). This is the first simulation that finds the expected multi-hadron states in this channel. However, the uncertainties on the extracted energies are sizable and the extracted $N\pi$ phase shift is consistent with zero within a large error.

One of our main results is that only three eigenstates lie below 1.65 GeV, while the fourth one lies already at about 1.8(1) GeV or higher. In contrast, the experimental $N\pi$ phase shift implies four lattice energy levels below 1.65 GeV in the elastic approximation when $N\pi$ is decoupled from $N\pi\pi$ and the later channel is noninteracting. Our results indicate that the low-lying Roper resonance does not arise on the lattice within the elastic approximation of $N\pi$ scattering. This points to a possibility of a dynamically generated resonance, where the coupling of $N\pi$ with $N\pi\pi$ or other channels is essential for the existence of this resonance. This is supported by comparable overlaps of the operator $O^{N\sigma}$ to the second and third eigenstates.

We come to a similar conclusion if we compare our lattice spectrum to the HEFT predictions for $N\pi/N\sigma/\Delta\pi$ scattering in three scenarios [8]. The case where these three channels are coupled with the low-lying bare Roper qqq core is disfavored. Our results favor the scenario where the Roper resonance arises solely as a coupled channel phenomenon, without the Roper qqq core.

Future steps towards a better understanding of this channel include simulations at larger $m_\pi L$, decreasing the statistical error and employing qqq or $qqqq\bar{q}$ operators with greater variety of spatially extended structures. Simulating the system at nonzero total momentum will give further information but will introduce additional challenges: states of positive as well as negative parity contribute to the relevant irreducible representations in this case. It would also be important to investigate the spectrum based on fermions with exact chiral symmetry at finite lattice spacing.

Our results point towards the possibility that Roper resonance is a coupled-channel phenomenon. If this is the case, the rigorous treatment of this channel on the lattice will be challenging. This is due to the three-hadron decay channel $N\pi\pi$ and the fact that the three-hadron scattering matrix has never been extracted from lattice QCD calculations yet. The simplified two-body approach to coupled channels $N\sigma/\Delta\pi$ (based on stable σ and Δ) cannot be compared quantitatively to the lattice data at light m_π where σ and Δ are broad unstable resonances. This is manifested also in our simulation, where the $O^{N\sigma}$ operator renders an eigenstate with $E \simeq m_N + 2m_\pi$ and not $E \simeq m_N + m_\sigma$.

Pion-nucleon scattering has been the prime source of our present day knowledge on hadrons. After decades of lattice QCD calculations we are now approaching the possibility to study that scattering process from first principles. This has turned out to be quite challenging and our contribution is only one step of more to follow.

ACKNOWLEDGMENTS

We thank the Parallel Array Computer System for Computational Sciences (PACS-CS) collaboration for providing the gauge configurations. We would kindly like to thank M. Döring, L. Glozman, Keh-Fei Liu and D. Mohler for valuable discussions. We are grateful to B. Golli, M. Rosina and S. Širca for careful reading of the manuscript and numerous valuable discussions and suggestions. This work is supported in part by the Slovenian Research Agency ARRS, by the Austrian Science Fund FWF:I1313-N27 and by the Deutsche Forschungsgemeinschaft Grant No. SFB/TRR 55. The calculations were performed on computing clusters at the University of Graz (NAWI Graz) and Ljubljana. S. P. acknowledges support from U.S. Department of Energy Contract No. DE-AC05-06OR23177, under which Jefferson Science Associates, LLC, manages and operates Jefferson Lab.

APPENDIX A: AN EXAMPLE OF A WICK CONTRACTION

Here an example of a Wick contraction is sketched in order to illustrate how one deals with the spin components at the source and sink. Let us consider the correlation function for the first $n\pi^+$ term in $O^{N\pi,m_s=1/2}$ at the sink and $O^{N,m_s=1/2}$ at the source (7):

$$\begin{aligned}\langle n_{-1/2}(-e_x)\pi^+(e_x)|p_{1/2}(0)\rangle &= \langle (u^T\Gamma_2 d)(\Gamma_1 d)_{\mu=2}(\bar{d}\gamma_5 u)|(\bar{u}\Gamma'_1)_{\mu'=1}(\bar{d}\Gamma'_2\bar{u})\rangle \\ &= \langle u_\alpha(\Gamma_2)_{\alpha\beta}d_\beta(\Gamma_1 d)_\mu \bar{d}_\gamma(\gamma_5)_{\gamma\delta}u_\delta|(\bar{u}\Gamma'_1)_{\mu'}\bar{d}_{\alpha'}(\Gamma'_2)_{\alpha'\beta'}\bar{u}_{\beta'}\rangle \\ &= -(\Gamma_1 d\bar{d})_{\mu\gamma}(\Gamma_2)_{\alpha\beta}(\Gamma'_2)_{\alpha'\beta'}(\gamma_5)_{\gamma\delta}(d\bar{d})_{\beta\alpha'}(u\bar{u})_{\delta\beta'}(u\bar{u}\Gamma'_1)_{\alpha\mu'} + \text{three contractions} \\ &= M_{\mu\mu'} + \text{three contractions} = M_{21} + \text{three contractions}. \end{aligned} \tag{A1}$$

Among four Wick contractions one is shown as an example: there $\bar{d}$ from the pion at the sink contracts with $(\Gamma_1 d)_\mu$ from the neutron at the sink, while the remaining quark lines follow a standard proton contraction. All indices except for Dirac indices are omitted for simplicity.

The open Dirac-spinor index is $\mu' = 1$ at the source and $\mu = 2$ at the sink for this particular term, while all other Dirac indices are summed over. The open indices μ and μ' can be represented in the matrix form $M_{\mu\mu'}$ where the element M_{21} is relevant for the given contraction. Any Wick contraction in our correlation matrix can be represented by some matrix $M_{\mu\mu'}$, where $\mu' = 1$ ($\mu' = 2$) is taken for nucleon with spin up (down) in the source, and $\mu = 1$ ($\mu = 2$) for nucleon with spin up (down) in the sink.

APPENDIX B: MORE ON THE EFFECTIVE ENERGIES

The effective energies for various choices of interpolator and configuration sets are presented in Fig. 9.

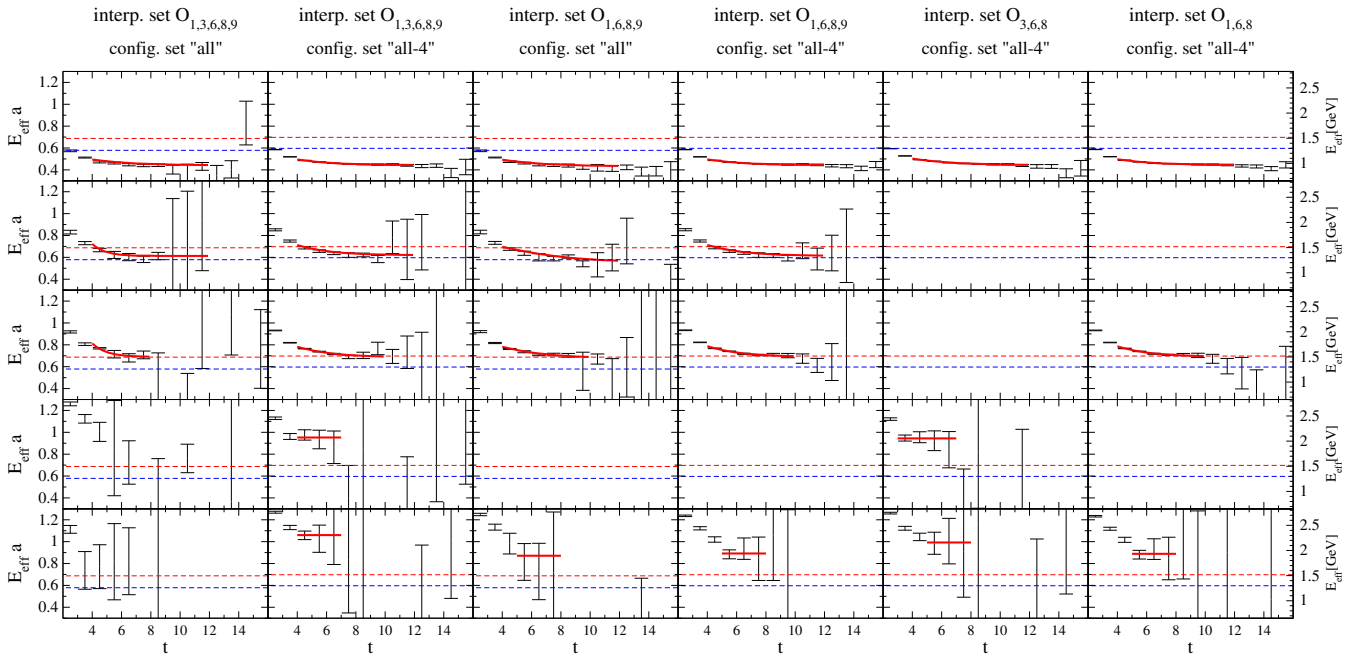

FIG. 9. Effective energies $E_n^{\text{eff}}(t)$ for various choices of interpolator sets and configuration sets, that are discussed in Sec. II A. The dashed horizontal lines present noninteracting energies of $N(0)\pi(0)\pi(0)$ (blue dashed) and $N(1)\pi(-1)$ (red dashed) for the corresponding configuration sets. The fit estimates are shown as red solid curves. The highest energy levels lie near or above 2 GeV and we refrain from fitting those since no clear plateau is observed.

[1] K. A. Olive *et al.* (Particle Data Group), Chin. Phys. C **38**, 090001 (2014).
[2] L. D. Roper, Phys. Rev. Lett. **12**, 340 (1964).
[3] N. Isgur and G. Karl, Phys. Rev. D **18**, 4187 (1978).
[4] K. F. Liu and C. W. Wong, Phys. Rev. D **28**, 170 (1983).
[5] S. Capstick and N. Isgur, Phys. Rev. D **34**, 2809 (1986).
[6] O. Krehl, C. Hanhart, S. Krewald, and J. Speth, Phys. Rev. C **62**, 025207 (2000).
[7] C. Schutz, J. Haidenbauer, J. Speth, and J. W. Durso, Phys. Rev. C **57**, 1464 (1998).
[8] Z.-W. Liu, W. Kamleh, D. B. Leinweber, F. M. Stokes, A. W. Thomas, and J.-J. Wu, arXiv:1607.04536.
[9] A. Matsuyama, T. Sato, and T. S. H. Lee, Phys. Rep. **439**, 193 (2007).
[10] R. Jaffe and F. Wilczek, Eur. Phys. J. C **33**, S38 (2004).
[11] B. Julia-Diaz and D. O. Riska, Nucl. Phys. **A780**, 175 (2006).
[12] E. Golowich, E. Haqq, and G. Karl, Phys. Rev. D **28**, 160 (1983); **33**, 859(E) (1986).
[13] L. S. Kisslinger and Z. P. Li, Phys. Rev. D **51**, R5986 (1995).
[14] L. Y. Glozman and D. O. Riska, Phys. Rep. **268**, 263 (1996).
[15] L. Y. Glozman, W. Plessas, K. Varga, and R. Wagenbrunn, Phys. Rev. D **58**, 094030 (1998).
[16] P. Alberto, M. Fiolhais, B. Golli, and J. Marques, Phys. Lett. B **523**, 273 (2001).
[17] B. Golli and S. Sirca, Eur. Phys. J. A **38**, 271 (2008).
[18] M. Hoferichter, J. Ruiz de Elvira, B. Kubis, and U.-G. Meißner, Phys. Rep. **625**, 1 (2016).
[19] A. L. Kiratidis, W. Kamleh, D. B. Leinweber, Z.-W. Liu, F. M. Stokes, and A. W. Thomas, arXiv:1608.03051.
[20] M. Lüscher, Nucl. Phys. **B354**, 531 (1991).
[21] M. Lüscher, Nucl. Phys. **B364**, 237 (1991).
[22] K.-F. Liu, Y. Chen, M. Gong, R. Sufian, M. Sun, and A. Li, *Proc. Sci.*, LATTICE2013 (2014) 507 [arXiv:1403.6847].
[23] C. Alexandrou, T. Korzec, G. Koutsou, and T. Leontiou, Phys. Rev. D **89**, 034502 (2014).
[24] C. Alexandrou, T. Leontiou, C. N. Papanicolas, and E. Stiliaris, Phys. Rev. D **91**, 014506 (2015).
[25] G. P. Engel, C. B. Lang, D. Mohler, and A. Schaefer, Phys. Rev. D **87**, 074504 (2013).
[26] R. G. Edwards, J. J. Dudek, D. G. Richards, and S. J. Wallace, Phys. Rev. D **84**, 074508 (2011).
[27] M. S. Mahbub, W. Kamleh, D. B. Leinweber, P. J. Moran, and A. G. Williams, Phys. Rev. D **87**, 094506 (2013).
[28] D. S. Roberts, W. Kamleh, and D. B. Leinweber, Phys. Lett. B **725**, 164 (2013).
[29] D. Leinweber, W. Kamleh, A. L. Kiratidis, Z.-W. Liu, S. Mahbub, D. Roberts, F. Stokes, A. W. Thomas, and J.-J. Wu, J. Phys. Soc. Jpn. Conf. Proc. **10**, 010011 (2016).
[30] K.-F. Liu, arXiv:1609.02572.
[31] C. Liu, arXiv:1612.00103.
[32] D. S. Roberts, W. Kamleh, and D. B. Leinweber, Phys. Rev. D **89**, 074501 (2014).
[33] N. Mathur, Y. Chen, S. J. Dong, T. Draper, I. Horváth, F. X. Lee, K. F. Liu, and J. B. Zhang, Phys. Lett. B **605**, 137 (2005).
[34] M. S. Mahbub, A. Ó. Cais, W. Kamleh, B. G. Lasscock, D. B. Leinweber, and A. G. Williams, Phys. Lett. B **679**, 418 (2009).
[35] M. Doring, U.-G. Meissner, E. Oset, and A. Rusetsky, Eur. Phys. J. A **47**, 139 (2011).
[36] M. T. Hansen and S. R. Sharpe, Phys. Rev. D **86**, 016007 (2012).
[37] J. J. Dudek, R. G. Edwards, C. E. Thomas, and D. J. Wilson, Phys. Rev. Lett. **113**, 182001 (2014).
[38] J. J. Dudek, R. G. Edwards, and D. J. Wilson (Hadron Spectrum Collaboration), Phys. Rev. D **93**, 094506 (2016).
[39] M. T. Hansen and S. R. Sharpe, Phys. Rev. D **92**, 114509 (2015).
[40] S. Aoki *et al.*, Phys. Rev. D **79**, 034503 (2009).
[41] C. B. Lang and V. Verduci, Phys. Rev. D **87**, 054502 (2013).
[42] V. Verduci and C. B. Lang, *Proc. Sci.*, LATTICE2014 (2014) 121 [arXiv:1412.0701].
[43] P. H. Ginsparg and K. G. Wilson, Phys. Rev. D **25**, 2649 (1982).
[44] C. Michael, Nucl. Phys. **B259**, 58 (1985).
[45] M. Lüscher, Commun. Math. Phys. **104**, 177 (1986).
[46] M. Lüscher and U. Wolff, Nucl. Phys. **B339**, 222 (1990).
[47] B. Blossier, M. Della-Morte, G. von Hippel, T. Mendes, and R. Sommer, J. High Energy Phys. 04 (2009) 094.
[48] M. Peardon, J. Bulava, J. Foley, C. Morningstar, J. Dudek, R. G. Edwards, B. Joó, H.-W. Lin, D. G. Richards, and K. Jimmy Juge (Hadron Spectrum Collaboration), Phys. Rev. D **80**, 054506 (2009).
[49] C. Morningstar, J. Bulava, J. Foley, K. J. Juge, D. Lenkner, M. Peardon, and C. H. Wong, Phys. Rev. D **83**, 114505 (2011).
[50] C. B. Lang, D. Mohler, S. Prelovsek, and M. Vidmar, Phys. Rev. D **84**, 054503 (2011).
[51] S. Prelovsek, U. Skerbis, and C. B. Lang, arXiv: 1607.06738 [J. High Energy Phys. (to be published)].
[52] R. A. Briceno, J. J. Dudek, R. G. Edwards, and D. J. Wilson, Phys. Rev. Lett. **118**, 022002 (2017).
[53] M. Göckeler, R. Horsley, M. Lage, U.-G. Meißner, P. E. L. Rakow, A. Rusetsky, G. Schierholz, and J. M. Zanotti, Phys. Rev. D **86**, 094513 (2012).
[54] D. Brömmel, P. Crompton, C. Gattringer, L. Glozman, C. Lang, S. Schaefer, and A. Schäfer, Phys. Rev. D **69**, 094513 (2004).
[55] R. L. Workman, R. A. Arndt, W. J. Briscoe, M. W. Paris, and I. I. Strakovsky, Phys. Rev. C **86**, 035202 (2012).
[56] gwdac.phys.gwu.edu.
[57] M. T. Hansen and S. R. Sharpe, arXiv:1609.04317 [Phys. Rev. D (to be published)].
[58] Z.-p. Li, V. Burkert, and Z.-j. Li, Phys. Rev. D **46**, 70 (1992).
[59] V. I. Mokeev *et al.* (CLAS Collaboration), Phys. Rev. C **86**, 035203 (2012).
[60] R. F. Lebed, Phys. Lett. B **749**, 454 (2015).